Electronic Supplementary Information

Fe(II)-assisted One-pot Synthesis of Ultra-small Core-shell Au-Pt Nanoparticles as Superior Catalysts towards HER and ORR

Yi Cao,[†] Yujiao Xiahou,[†] Lixiang Xing,[†] Xiang Zhang,[†] Hong Li,[†] Chenshuo Wu,[†] and Haibing Xia [†]*

†State Key Laboratory of Crystal Materials, Shandong University, Jinan, 250100, P. R. China.

Figure S1. The RHE calibration was performed in the high purity hydrogen saturated electrolyte with a Pt foil as the working electrode. Cyclic voltammetry (CV) was run at a scan rate of 5 $mV \cdot s^{-1}$, and the average of the two potentials at which the current crossed zero was taken to be the thermodynamic potential for the hydrogen electrode reactions.

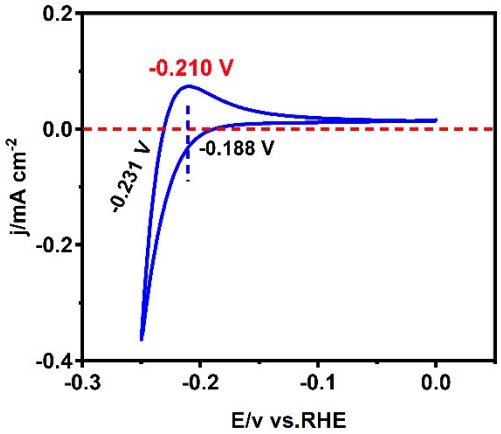

Figure S2. TEM image of Au NPs prepared by the same procedure used for synthesis of USCS Au-Pt NPs but in the absence of Pt precursors. The concentrations of Fe(II) ions, Au(III) ions, and citrate used for synthesis of Au NPs were 0.130, 0.015, and 0.687 mm, respectively.

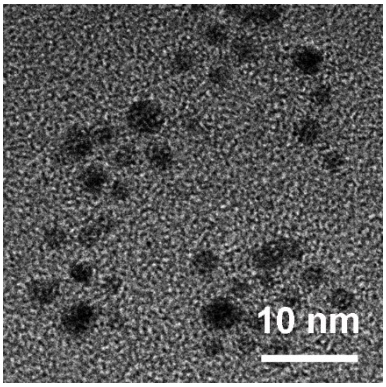

It is found that the resulting pure Au NPs show a broad distribution in size and shape, indicating that the newly formed Au cores could be not sufficiently stabilized by citrate.

Figure S3. Digital photographs of the colors of the solutions of Au precursors before and after reacting with Fe(II) ions (a) and citrate (b) at room temperature (25 °C), respectively.

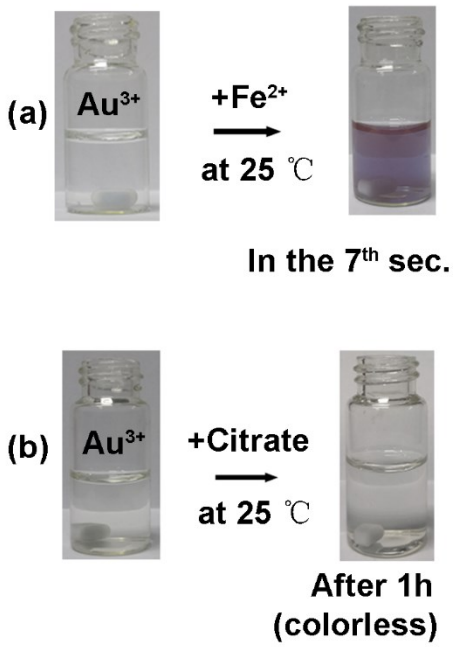

Since the solution of the formed Au NPs can show colors due to their special plasmonic character, the colors of their solution can help us to determine the formation of Au NPs. As shown in Fig. S3a, after the addition of Fe(II) ions solution into the solution of Au(III) ions at room temperature, the color of the mixture solution changed instantaneously and can keep unchanged after 7 seconds, indicating the formation of Au NPs within 7 seconds. However, there was no color change observed after the addition of citrate solution into the solution of Au(III) ions at room temperature. And the color of the mixture solution was still unchanged after stirring for 1 hour at room temperature (Fig. S3b). Thus, the results indicate that the chemical reaction between Au(III) ions and Fe(II) ions ($Au^{3+} + 3Fe^{2+} \rightarrow Au^{0} + 3Fe^{3+}$) is indeed faster than that between Au(III) ions and citrate.

Figure S4. Digital photographs of the colors of the solutions of Pt precursors reacting with Fe(II) ions at 25 °C.

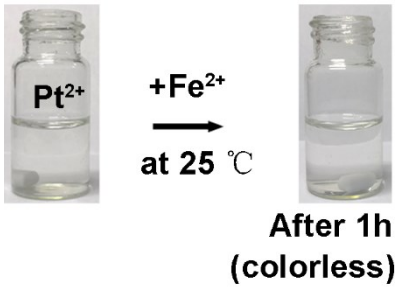

One can see that there was no color change observed after the addition of the solution of Fe(II) ions into the solution of Pt(II) ions at room temperature (at 25 °C). In addition, the color of the mixture solution was still unchanged after stirring for 1 hour at room temperature (Fig. S4). Thus, the result indicates that the chemical reaction between Pt(II) ions and Fe(II) ions ($Pt^{2+} + 2Fe^{2+} \rightarrow Pt^{0} + 2Fe^{3+}$) is rather slower than that between Au(III) ions and Fe(II) ions, compared with the results of the reactions between Au(III) ions and Fe(II) ions (Fig. S3a).

Figure S5. Digital photographs of the colors of the solutions of Pt precursors before and after reacting with Fe(II) ions (a) and citrate (b) at 100 °C, respectively.

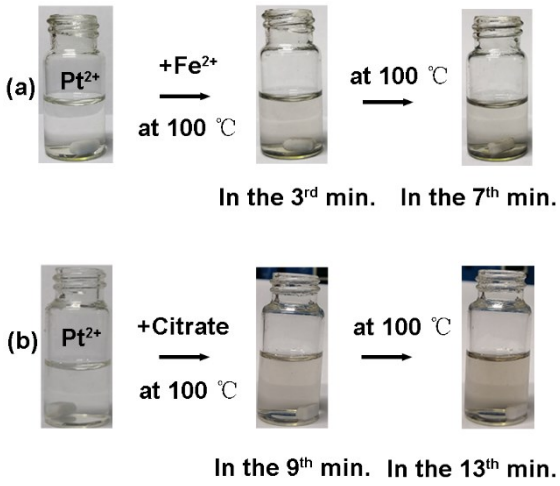

The color of the solution of Pt(II) ions after the addition of Fe(II) ions began to appear pale yellow ($Pt^{2+} + 2Fe^{2+} \rightarrow Pt^{0} + 2Fe^{3+}$) at the 3rd minute at 100 °C (Fig. S5a), which was significantly faster than that of Pt precursors after the addition of citrate ions at 100 °C (Fig. S5b). Thus, the reducing ability of citrate is weaker than Fe(II) ions. Combined with the results described earlier (Fig. S3 and S4), one can conclude that both the Pt(II) ions and Au(III) ions in the solution are mainly reduced by Fe(II) ions. And the citrate mainly acts as a stabilizer in the course of synthesis.

Figure S6. TEM image (a) and HAADF-STEM-EDS mapping images (b to d) of AuPt alloyed NWNs (A). CO stripping voltammogram of AuPt alloyed NWNs (B), measured in a N_2-saturated 0.5 M H_2SO_4 at 50 mV s^{-1}. CO stripping voltammogram of USCS $Au_{38.4}@Au_{9.3}Pt_{52.3}$ NPs was also given (black curve in B) for better comparison.

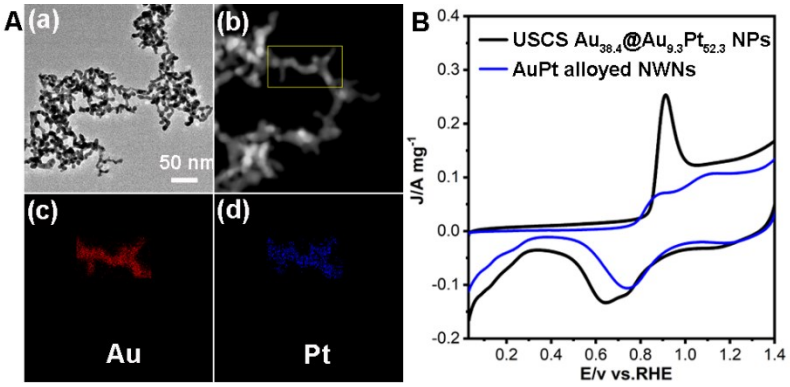

AuPt alloyed nanowire-networks (NWNs) as a reference sample were prepared as follows. Firstly, an aqueous solution of $HAuCl_4$ (0.5 mL, 25 mM) was added into the freshly prepared citrate solution (1.0 mL, 34.3 mM). After stirring of 12 min at room temperature, Au NWNs with an average diameter of 3 nm (3 nm Au NWNs) were formed in the solution, followed by the centrifugation (at 16000 rcf for 4 min) to remove the supernatant and the re-dispersion of them in water. Then, an aqueous solution of HCl (60 μL, 0.1 M) was added into an aqueous dispersion of 3 nm Au NWNs (0.5 mL, 5 mM), followed by the addition of an aqueous solution of K_2PtCl_6 (0.169 mL, 1.286 mM) under vigorous stirring. Next, after the above mixture was heated to 80 °C within 2 min under stirring, an aqueous solution of AA (0.2 mL, 0.1 M) was injected after the heating of 30 min, followed by the incubation of 4 h at 80 °C under stirring. Eventually, AuPt alloyed NWNs were collected by three repeated rounds of the centrifugation (at 6000 rcf for 5 min) and the washing by Milli-Q water.

The morphology and composition of the as-prepared AuPt alloyed NWNs were characterized by TEM and HAADF-STEM-EDS mapping images (Fig. S6A). The uniform distribution of Au and Pt elements demonstrates the formation of an alloy structure (Fig. S6A-c and S6A-d). In addition, the CO stripping voltammogram of the as-prepared AuPt alloyed NWNs was performed for better comparison (blue curve in Fig. S6B). One can clearly see that a broader CO oxidation peak appears in the CO stripping voltammogram of AuPt alloyed NWNs (blue curve in Fig. S6B), which is consistent with those reported in literature.[1] In contrast, the pronounced and sharp CO oxidation peak was observed in the CO stripping voltammogram of USCS $Au_{38.4}@Au_{9.3}Pt_{52.3}$ NPs, indicating that the surfaces of USCS $Au_{38.4}@Au_{9.3}Pt_{52.3}$-NP/C catalysts possess continuous Pt atoms (like commercial Pt/C catalysts)[2] and their surfaces are not the Au-Pt alloyed surfaces (Fig. S6),[1] but Au-decorated Pt surfaces (namely the Pt-rich shells have an Au-decorated Pt surfaces).

Figure S7. CO stripping voltammograms of 6 nm Au NPs (a) and intermediate products of USCS $Au_{38.4}@Au_{9.3}Pt_{52.3}$ NPs at different reaction times: 3 s (b), 2 min (c), 5 min (d), and 30 min (e); They measured in N_2-saturated 0.5 M H_2SO_4 at 5 mV s^{-1}.

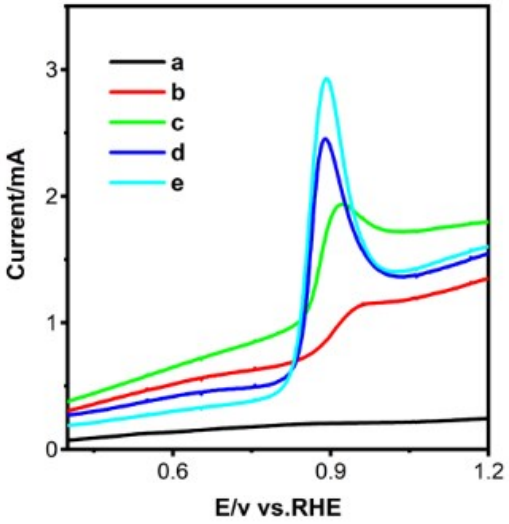

CO stripping voltammograms of 6 nm pure Au NPs, intermediate products during the formation of USCS $Au_{38.4}@Au_{9.3}Pt_{52.3}$ NPs and final USCS $Au_{38.4}@Au_{9.3}Pt_{52.3}$ NPs were investigated for comparison (Fig. S7). In CO stripping voltammogram of 6 nm pure Au NPs, there is hardly any obvious CO oxidation peak (Fig. S7a), indicating that pure gold would not contribute to CO adsorption.[3] However, with the increasing Pt ratio in intermediate products, their CO oxidation peaks become more obvious. In addition, the shapes of these peaks evolve from broad to sharp and their center positions also negatively shifted (Fig. S7b to d).[4] In contrast, CO oxidation peak of the USCS $Au_{38.4}@Au_{9.3}Pt_{52.3}$ NPs bear the sharpest shape and the most negative potential (Fig. S7e), which is obviously different from those with alloy Au-Pt surfaces (Fig. S6). Note that even if at the initial stage (Fig. S7b), a broad CO peaks exists, instead of a diffuse CO peaks. This result indicates that the as-formed Au-Pt nanoparticles during the whole process are not the alloyed Au-Pt nanoparticles (Fig. S6). Moreover, the results also indicate that the ratio of Au at the outer shell of intermediate products during the formation of USCS Au-Pt NPs gradually decreases while the ratio of Pt at the outer shell of intermediate products increases. Thus, taken EDS results and CO striping results together, USCS $Au_{38.4}@Au_{9.3}Pt_{52.3}$ NPs bear the structure of Au-rich core and Pt-rich shell. In addition, the Pt-rich shell has an Au-decorated Pt surface, instead of an Au-Pt alloy surface.

Figure S8. CV curves of the GCEs modified by USCS $Au_{38.4}@Au_{9.3}Pt_{52.3}$ NPs in 0.5 M N_2-saturated H_2SO_4 solution at room temperature. The regions denoted by the horizontal segments were used to calculate the surface areas of Pt and Au, using the surface charge associated with the reduction of their oxide.

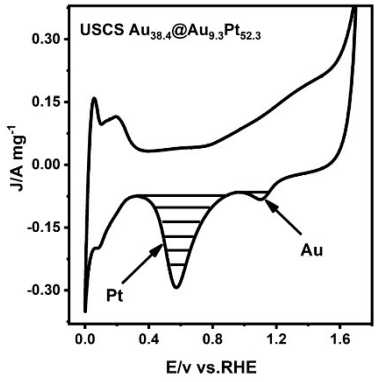

The whole NP composition and surface composition of USCS Au-Pt NPs were determined by using cyclic voltammetry in an acidic medium, which have been used by our work[5] and others.[6] The charge associated to the desorption of oxide species can be used to determine the surface composition. The peak at 1.1 V vs. RHE and at 0.6 V vs. RHE during the negative going scan is associated to the reduction of Au oxide species and Pt oxide species, respectively (Fig. S8). For pure materials the charge associated to the reduction of oxide species are 493 mC cm^{-2} and 543 mC cm^{-2} for Au and Pt, respectively. The atomic content of Au can be deduced as follows:

$$m=\frac{S_{Au}}{S_{Au}+S_{Pt}}\times 100\%$$

where m represents the Au content, and S_{Au} and S_{Pt} are the surface covered by Au and Pt oxides, respectively. Table S4 displays the total and surface compositions of USCS $Au_{38.4}@Au_{9.3}Pt_{52.3}$ NPs obtained by ICP-MS and CV curve. The atomic fractions of Pt and Au in the shells and the Au in the cores can be deduced to 52.3 at%, 9.3 at%, and 38.4 at% for the USCS Au-Pt NPs. Thus, the composition of the as-prepared USCS Au-Pt NPs is determined to be USCS $Au_{38.4}@Au_{9.3}Pt_{52.3}$ NPs, which have the CS structure with Au-decorated Pt surfaces.

Figure S9. CV curves (A) and histograms (B) of the calculated ECSAs of the as-prepared USCS $Au_{38.4}$@$Au_{9.3}Pt_{52.3}$-NP/C catalysts (a) and commercial Pt/C (b) catalysts.

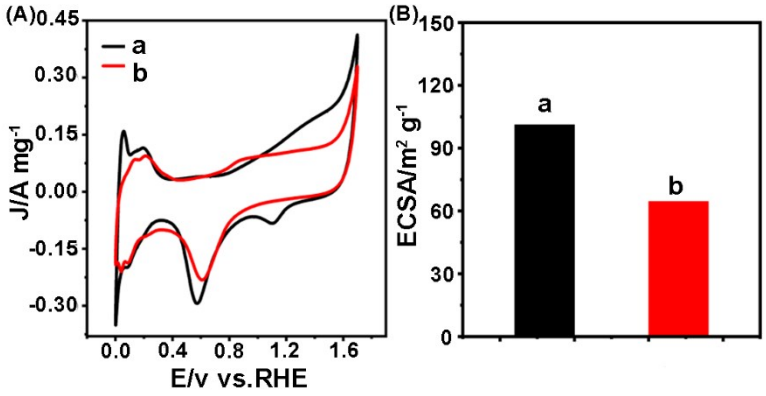

Figure S10. The HER LSV with a higher range in current density of the as-prepared USCS $Au_{38.4}@Au_{9.3}Pt_{52.3}$-NP/C catalysts and commercial Pt/C catalysts, measured in a N_2-saturated 0.5 M H_2SO_4 solution with a scan rate of 5 mV s^{-1}.

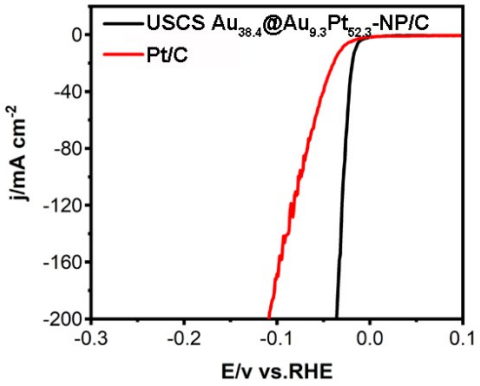

Figure S11. Chronoamperometric curves of the USCS $Au_{38.4}$@$Au_{9.3}Pt_{52.3}$-NP/C catalysts (a, black line) and commercial Pt/C catalysts (b, red line), measured at a potential of -33 mV (a, black line) and -40 mV (b, red line) for 10 h, respectively.

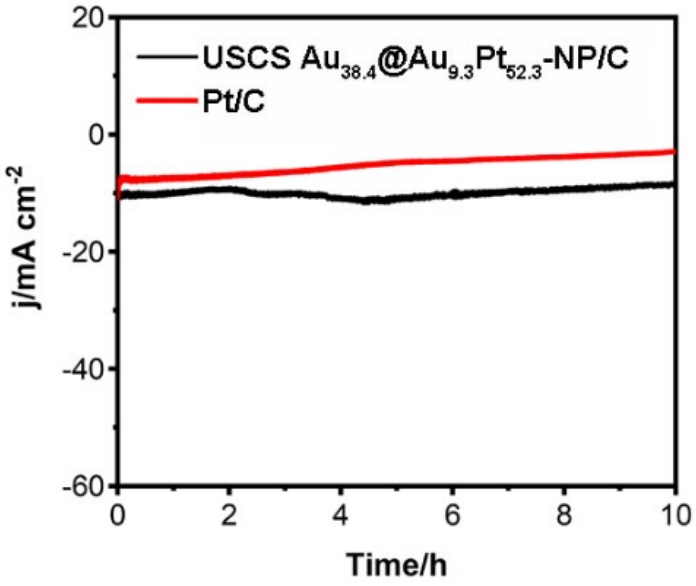

Figure S12. CO stripping voltammograms (a) of USCS $Au_{38.4}@Au_{9.3}Pt_{52.3}$-NP/C catalysts (black line) and commercial Pt/C catalysts (red line) performed in N_2-saturated 0.5 M H_2SO_4 at 50 mV s^{-1}; magnified current peaks (b) in CO stripping voltammograms.

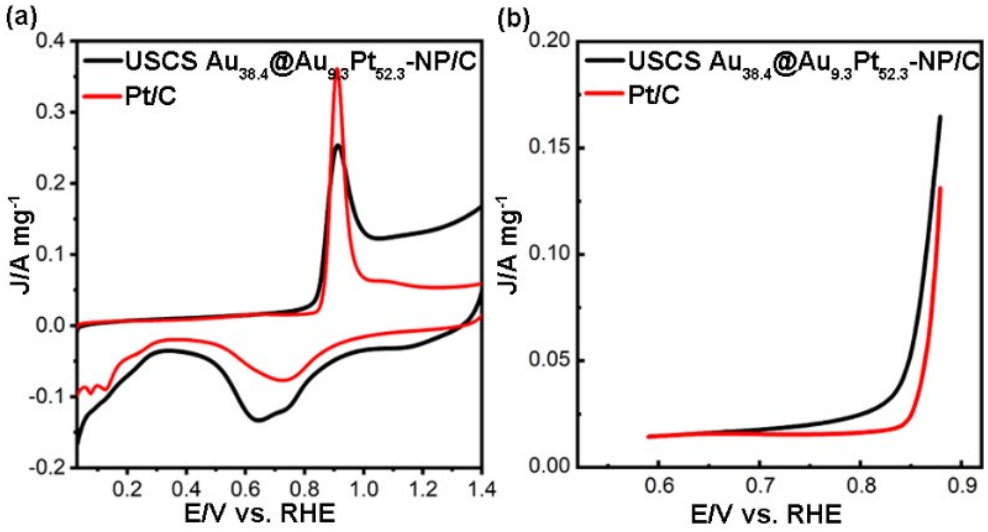

For better comparison, CO stripping voltammograms of USCS $Au_{38.4}@Au_{9.3}Pt_{52.3}$-NP/C catalysts (black line) and commercial Pt/C catalysts (red line) during the first stripping cycles are magnified and shown in Fig. S12b. The onset potential of CO oxidation of USCS $Au_{38.4}@Au_{9.3}Pt_{52.3}$-NP/C catalysts (black line) occurs at a less negative potential than that of commercial Pt/C catalysts, indicating an enhanced CO removal ability. The result indicates that USCS $Au_{38.4}@Au_{9.3}Pt_{52.3}$-NP/C catalysts may have a better desorption ability for oxides intermediates (such as CO and −OH).[7]

Figure S13. LSV curves of the as-prepared USCS $Au_{38.4}@Au_{9.3}Pt_{52.3}$-NP/C catalysts (a) and commercial Pt/C catalysts (b) towards ORR at a rotation rate from 400 to 1,600 rpm.

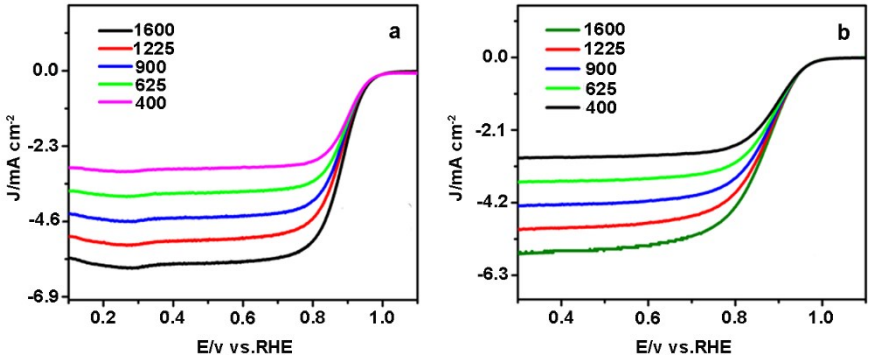

Figure S14. Histograms of the calculated mass- and specific activities at 0.85 V of the as-prepared USCS $Au_{38.4}@Au_{9.3}Pt_{52.3}$-NP/C catalysts (a) and commercial Pt/C catalysts (b) on the RDEs towards ORR in acidic media.

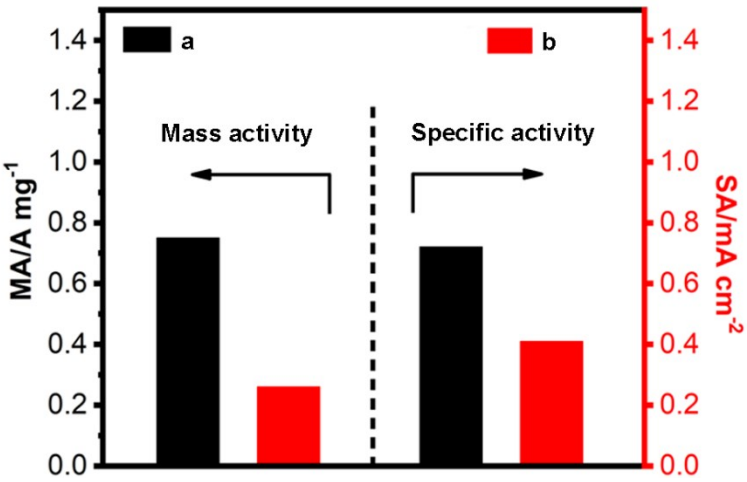

Figure S15. LSV curves of commercial Pt/C catalysts towards ORR before and after ADT. Their LSV curves were recorded in an O_2-saturated 0.1 M $HClO_4$ solution with a scan rate of 10 mV s^{-1} and a speed of 1,600 rpm.

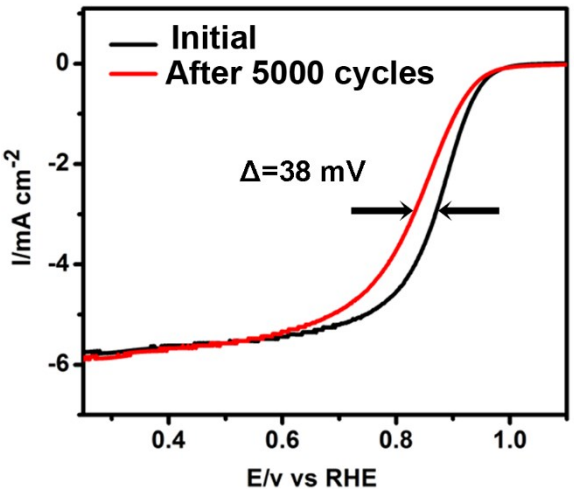

Table S1. Summarized binding energies of Pt 4f signals of USCS $Au_{38.4}@Au_{9.3}Pt_{52.3}$ NPs and pure Pt NPs.

Samples	Pt $4f_{5/2}$ peak [eV]	Pt $4f_{7/2}$ peak [eV]	ΔPt $4f_{7/2}$ peak [eV]
USCS $Au_{38.4}@Au_{9.3}Pt_{52.3}$ NPs	75.40	72.10	+1.25
Pure Pt NPs	74.20	70.85	0

Table S2. Summarized binding energies of Au 4f signals of USCS $Au_{38.4}@Au_{9.3}Pt_{52.3}$ NPs and pure Au NPs.

Samples	Au $4f_{5/2}$ peak [eV]	Au $4f_{7/2}$ peak [eV]	ΔAu $4f_{7/2}$ peak [eV]
USCS $Au_{38.4}@Au_{9.3}Pt_{52.3}$ NPs	87.25	83.65	-0.05
Pure Au NPs	87.30	83.70	0

Table S3 Summarized data of atomic ratio (at%) of Au and Pt in the intermediate products taken out at different reaction times during the formation of USCS $Au_{38.4}@Au_{9.3}Pt_{52.3}$ NPs by **EDS**. The reaction time in (a), (b), (c), and (d) is 3 s, 2 min, 5 min, and 30 min, respectively.

Sample	a	b	c	d
Au/at%	72	63	54	43
Pt/at%	28	37	46	57

A series of intermediates during the formation of USCS Au-Pt NPs were taken out to determine the atomic ratios of Au and Pt by EDS (Table S3). At the initial stage (a to c in Table S3), the atomic ratio of Au is bigger than that of Pt, indicating that the amount of Au is much more than that of Pt in the core part because Au cores can be formed firstly (within 7 s at room temperature) due to the preferential reduction of Au(III) ions by Fe(II) ions. In addition, after reaction of 5 min (d in Table S3), the ratio of Pt is bigger than that of Au instead, indicating that the amount of Pt is more than that of Au in the outer shell part of USCS Au-Pt NPs because the abundant Au precursors have been consumed after the formation of Au cores. Thus, the ratio of Pt-to-Au increases with the reaction time increasing, indicating the formation of the structure of Au-rich core and Pt-rich shell.

Table S4. Summarized data of the total and surface compositions of USCS $Au_{38.4}@Au_{9.3}Pt_{52.3}$ NPs obtained by **ICP-MS** and CV curve.

Sample	Total content		Surface content			
	Au(at%)	Pt(at%)	Au(at%)	Pt(at%)	m(Au%)	1-m(Pt%)
USCS $Au_{38.4}@Au_{9.3}Pt_{52.3}$ NPs	47.7	52.3	9.3	52.3	15.1	84.9

Table S5. Summarized particle sizes of Au-Pt NPs obtained at different concentrations of Fe(II) ions. The concentrations of Au(III) ions and Pt(II) ions were 0.015 mM and 0.024 mM, respectively.

concentration of Fe(II) ions [mM]	Particle size [nm]
0.013	2-6
0.060	2.9 ± 1.0
0.130	2.3 ± 0.5

Table S6. Summarized particle sizes of Au-Pt NPs obtained at different concentrations of Au(III) ions. The concentrations of Pt(II) ions and Fe(II) ions were 0.024 mM and 0.130 mM, respectively.

concentration of Au(III) ions [mM]	Particle size [nm]
0.015	2.3 ± 0.5
0.025	2.4 ± 0.7
0.050	2.6 ± 0.9
0.0625	2 - 5

Table S7. Summarized data of particle sizes and ECSAs of Au-Pt NPs obtained at different concentrations of Pt(II) ions. The concentrations of Au(III) ions and Fe(II) ions were 0.015 mM and 0.130 mM, respectively.

concentrations of Pt(II) ions [mM]	Particle size [nm]	ECSA[m^2g^{-1}]
0.014	2.2 ± 0.8	98.7
0.024	2.3 ± 0.5	101.2
0.034	2.5 ± 0.8	75.9

Table S8. Comparison of HER activity in acidic electrolyte of our sample with that of other catalysts reported in literature.

Catalysts	Overpotential at -10 $mAcm^{-2}$ [mV]	Tafel slop [$mV\ dec^{-1}$]	Mass activity @-0.05 V [$A \cdot mg_{Pt}^{-1}$]	Ref.
USCS $Au_{38.4}@Au_{9.3}Pt_{52.3}$-NP/C	16	14	49.7(@-0.04 V)	This work
PtW_6O_{24}/C	22	29.8	20.175(@-0.077 V)	8
Pt_4Co_1 HNPs	14.8	27.45	-	9
Pt SA/WO_{3-X}	38	45	12.8	10
PtRu dimers	-	28.9	23.1	11
EG-Pt/CoP-1.5	21	41	-	12
Pt/f-MWCNTs	43.9	30	18.16	13
GO/Au@Pt(<2nm)	-	39	-	14
β-$Ni_2P_2O_7$/Pt	28	32	-	15
Mo_2C@NC@Pt	27	28	-	16
Pt-FeNi@C		26.1	37.8	17
Pt/CNTs-ECR	34	26	-	18
PtNi/10PG CNCs	30.98	18	-	19
Pt/Fe–Au	43	30.6	-	20
CDs/Pt-PANI	30	41.7	-	21

Table S9. Comparison of ORR activity in acidic electrolyte of our sample with that of other catalysts reported in literature.

Catalysts	$E_{1/2}$ [mV]	Mass activity [$A \cdot mg_{Pt}^{-1}$]	Ref.
USCS $Au_{38.4}$@$Au_{9.3}Pt_{52.3}$-NP/C	0.896	0.75	This work
Pt@MoS_2/NrGO	0.895	-	22
Pt@NC/C	0.882	0.1165	23
NCNT-MLD-Pt	0.89	0.66	24
PtPd on graphitic nanofibers	-	0.42	25
PtPd@Pt core/satellite NAs	0.88	-	26
Pt-o-Cu_3Pt/C	-	0.64	27
$Pt_{0.8}Ni_{0.2}$/C	0.818	0.39	28
Pt NCs(1.4 nm)/OMC	0.809	0.423	29
PtCu NSs/C	0.893	0.42	30
$Pt_{71}Co_{29}$ LNFs	-	0.12829	31
3D $Pt_{77}Ni_{23}$	0.856	0.34	32
$Pt_{76}Au_{24}$NW/C	-	0.5	33
AuPt@Pt NCs	0.89	0.25	34

Reference

1 Y. Wu, Y. Zhao, J. Liu and F. Wang, *J. Mater. Chem. A*, 2018, **6**, 10700–10709.
2 Z. Wu, Y.-Q. Su, E. J. M. Hensen, X. Tian, C. You and Q. Xu, *J. Mater. Chem. A*, 2019, **7**, 26402–26409.
3 Y. Song, C. Bi, C. Wu, H. He, L. Huang, D. Wang and H. Xia, *J. Mater. Chem. A*, 2017, **5**, 18878–18887.
4 J. Lee, J. K. Yoo, J. Kim, Y. Sohn and C. K. Rhee, *Electrochimica Acta*, 2018, **290**, 244–254.
5 C. Bi, C. Feng, T. Miao, Y. Song, D. Wang and H. Xia, *Nanoscale*, 2015, **7**, 20105–20116.
6 A. Habrioux, W. Vogel, M. Guinel, L. Guetaz, K. Servat, B. Kokoh and N. Alonso-Vante, *Phys. Chem. Chem. Phys.*, 2009, **11**, 3573.
7 C. Wu, H. Li, H. He, Y. Song, C. Bi, W. Du and H. Xia, *ACS Appl. Mater. Interfaces*, 2019, **11**, 46902–46911.
8 F.-Y. Yu, Z.-L. Lang, L.-Y. Yin, K. Feng, Y.-J. Xia, H.-Q. Tan, H.-T. Zhu, J. Zhong, Z.-H. Kang and Y.-G. Li, *Nat. Commun.*, 2020, **11**, 490.
9 M. Wei, L. Huang, S. Huang, Z. Chen, D. Lyu, X. Zhang, S. Wang, Z. Q. Tian and P. K. Shen, *J. Catal.*, 2020, **381**, 385–394.
10 J. Park, S. Lee, H. Kim, A. Cho, S. Kim, Y. Ye, J. W. Han, H. Lee, J. H. Jang and J. Lee, *Angew. Chem. Int. Ed.*, 2019, **58**, 16038–16042.
11 L. Zhang, R. Si, H. Liu, N. Chen, Q. Wang, K. Adair, Z. Wang, J. Chen, Z. Song, J. Li, M. N. Banis, R. Li, T.-K. Sham, M. Gu, L.-M. Liu, G. A. Botton and X. Sun, *Nat. Commun.*, 2019, **10**, 4936.
12 J. Li, H.-X. Liu, W. Gou, M. Zhang, Z. Xia, S. Zhang, C.-R. Chang, Y. Ma and Y. Qu, *Energy Environ. Sci.*, 2019, **12**, 2298–2304.
13 J. Ji, Y. Zhang, L. Tang, C. Liu, X. Gao, M. Sun, J. Zheng, M. Ling, C. Liang and Z. Lin, *Nano Energy*, 2019, **63**, 103849.
14 L. D. Germano, V. S. Marangoni, N. V. V. Mogili, L. Seixas and C. M. Maroneze, *ACS Appl. Mater. Interfaces*, 2019, **11**, 5661–5667.
15 J. Theerthagiri, E. S. F. Cardoso, G. V. Fortunato, G. A. Casagrande, B. Senthilkumar, J. Madhavan and G. Maia, *ACS Appl. Mater. Interfaces*, 2019, **11**, 4969–4982.
16 J.-Q. Chi, J.-Y. Xie, W.-W. Zhang, B. Dong, J.-F. Qin, X.-Y. Zhang, J.-H. Lin, Y.-M. Chai and C.-G. Liu, *ACS Appl. Mater. Interfaces*, 2019, **11**, 4047–4056.
17 A. Fan, C. Qin, X. Zhang, J. Yang, J. Ge, S. Wang, X. Yuan, S. Wang and X. Dai, J. *Mater. Chem. A*, 2019, **7**, 24347–24355.
18 X. Bao, Y. Gong, Y. Chen, H. Zhang, Z. Wang, S. Mao, L. Xie, Z. Jiang and Y. Wang, *J. Mater. Chem. A*, 2019, **7**, 15364–15370.
19 J. Yang, G. Ning, L. Yu, Y. Wang, C. Luan, A. Fan, X. Zhang, Y. Liu, Y. Dong and X. Dai, *J. Mater. Chem. A*, 2019, **7**, 17790–17796.
20 X. Guo, X. Li, S. Kou, X. Yang, X. Hu, D. Ling and J. Yang, *J. Mater. Chem. A*, 2018, **6**, 7364–7369.
21 Q. Dang, Y. Sun, X. Wang, W. Zhu, Y. Chen, F. Liao, H. Huang and M. Shao, *Appl. Catal., B*, 2019, **257**, 117905.
22 S. Ramakrishnan, M. Karuppannan, M. Vinothkannan, K. Ramachandran, O. J. Kwon and D. J. Yoo, *ACS Appl. Mater. Interfaces*, 2019, **11**, 12504–12515.

23 J. Liu, W. Li, R. Cheng, Q. Wu, J. Zhao, D. He and S. Mu, *Langmuir*, 2019, **35**, 2580−2586.
24 L. Zhang, Y. Zhao, M. Norouzi Banis, K. Adair, Z. Song, L. Yang, M. Markiewicz, J. Li, S. Wang, R. Li, S. Ye and X. Sun, *Nano Energy*, 2019, **60**, 111-118.
25 Y.-X. Xiao, J. Ying, G. Tian, Y. Tao, H. Wei, S.-Y. Fan, Z.-H. Sun, W.-J. Zou, J. Hu, G.-G. Chang, W. Li, X.-Y. Yang and C. Janiak, *Appl. Catal.*, *B*, 2019, **259**, 118080.
26 Y. Chen, G. Fu, Y. Li, Q. Gu, L. Xu, D. Sun and Y. Tang, *J. Mater. Chem. A*, 2017, **5**, 3774–3779.
27 N. Cheng, L. Zhang, S. Mi, H. Jiang, Y. Hu, H. Jiang and C. Li, *ACS Appl. Mater. Interfaces*, 2018, **10**, 38015–38023.
28 J. Liu, J. Lan, L. Yang, F. Wang and J. Yin, *ACS Sustain. Chem. Eng.*, 2019, **7**, 6541–6549.
29 J. Liu, X. Wu, L. Yang, F. Wang and J. Yin, *Electrochim. Acta*, 2019, **297**, 539-544.
30 W. Li, Z.-Y. Hu, Z. Zhang, P. Wei, J. Zhang, Z. Pu, J. Zhu, D. He, S. Mu and G. Van, *J. Catal.*, 2019, **375**, 164-170.
31 L. Zhang, X.-F. Zhang, X.-L. Chen, A.-J. Wang, D.-M. Han, Z.-G. Wang and J.-J. Feng, *J. Colloid Interface Sci.*, 2019, **536**, 556–562.
32 S. Fu, C. Zhu, J. Song, M. H. Engelhard, Y. He, D. Du, C. Wang and Y. Lin, *J. Mater. Chem. A*, 2016, **4**, 8755–8761.
33 F. Chang, S. Shan, V. Petkov, Z. Skeete, A. Lu, J. Ravid, J. Wu, J. Luo, G. Yu, Y. Ren and C.-J. Zhong, *J. Am. Chem. Soc.*, 2016, **138**, 12166–12175.
34 L. Zhang, S. Yu, J. Zhang and J. Gong, *Chem. Sci.*, 2016, **7**, 3500–3505.